Continuum Methods for Gyrokinetic Edge Plasma Simulation: COGENT

Numerical Methods for Kinetic Equations of Plasma Physics

3 Sep 2013, Max-Planck-Institut für Plasmaphysik, Garching bei München

J. A. F. Hittinger, M. R. Dorr (LLNL); P. Colella, P. McCorquodale (LBNL)

Lawrence Livermore National Laboratory

LLNL-PRES-642890

This work was performed under the auspices of the U.S. Department of Energy by Lawrence Livermore National Laboratory under Contract DE-AC52-07NA27344. Lawrence Livermore National Security, LLC

The Edge Simulation Laboratory is a collaboration between the ASCR and FES theory programs

- Goal: Develop continuum edge simulation numerical methodologies
- Motivated by FES interest in a continuum alternative to a particle-based approaches

- Applied Math: (Funded by US DOE ASCR)
  - Milo Dorr and Jeff Hittinger (LLNL)
  - Phil Colella and Peter McCorquodale (LBNL)
- Physics: (Funded by US DOE FES)
  - Ron Cohen, Tom Rognlien, Mikhail Dorf, John Compton (LLNL Fusion Energy Program)
  - Phil Snyder, Jeff Candy, Emily Belli (General Atomics)
  - Sergei Krasheninnikov, Justin Angus (UCSD)

Simulation of edge plasma turbulence in tokamak fusion reactors requires kinetic models

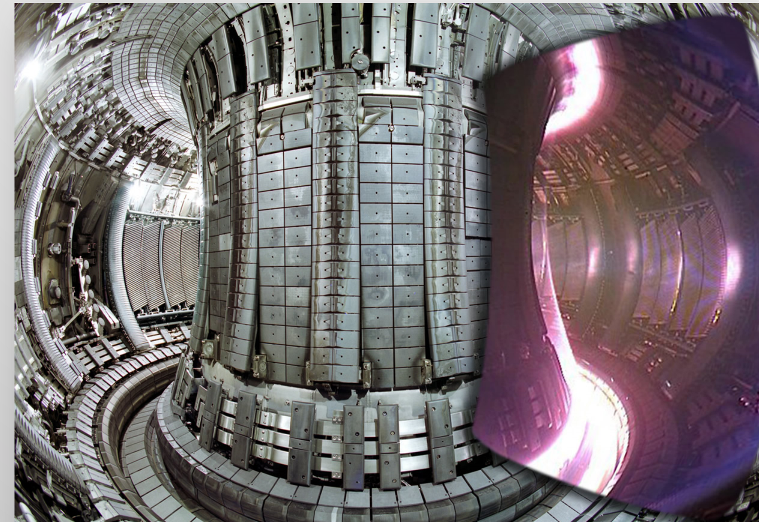

Image: EFDA-JET

- In high-performance (H-mode) discharges, a steep-gradient region (the pedestal) develops
  - Pedestal becomes a transport barrier
  - Kinetic models are required to model the pedestal evolution
- Extension to the plasma edge of continuum gyrokinetic models requires new algorithms to satisfy demanding requirements

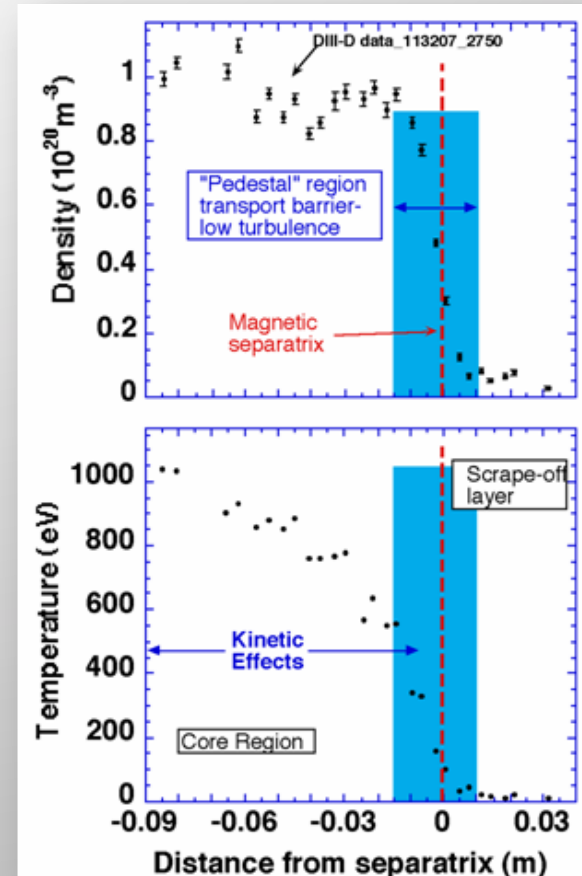

[G.D. Porter, et al., Phys. Plasmas 7 (2000)]

Gyrokinetic models are well established in plasma physics, but raise new challenges for edge simulation

- Kinetic models describe the evolution of distribution functions phase space

$$f(x, v, t) : \mathbb{R}^D \times \mathbb{R}^D \times [0, \infty) \rightarrow \mathbb{R}^+$$

- Gyrokinetic models decouple the gyromotion
  - Average gyro-motion is like propagating ring charges instead of point charges
  - Reduces 6D phase space to 5D
  - Removes a fast time scale

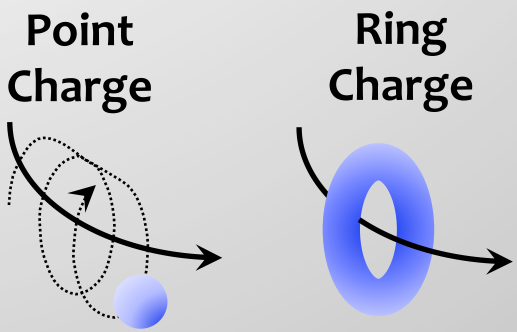

- Used to simulate core turbulence for many years
- Plasma edge differs from the core
  - Can not use perturbation formulation
  - Strong, rapidly varying density and temperature in pedestal yields overlapping time scales
  - More complicated geometry
  - Strong collisions towards the wall
- Highly anisotropic flow encourages magnetic-field-aligned grids

COGENT is solving the Hahm '96 model in a 4D divertor geometry

Gyrokinetic Vlasov:

$$\frac{\partial}{\partial_t}(B_\parallel^* f) + \nabla_R(\dot{\mathbf{R}} B_\parallel^* f) + \frac{\partial}{\partial_{v_\parallel}}(\dot{v}_\parallel B_\parallel^* f) = 0$$

describes the evolution of a distribution function

$$f \equiv f(\mathbf{R}, v_\parallel, \mu, t)$$

in gyrocenter phase space coordinates

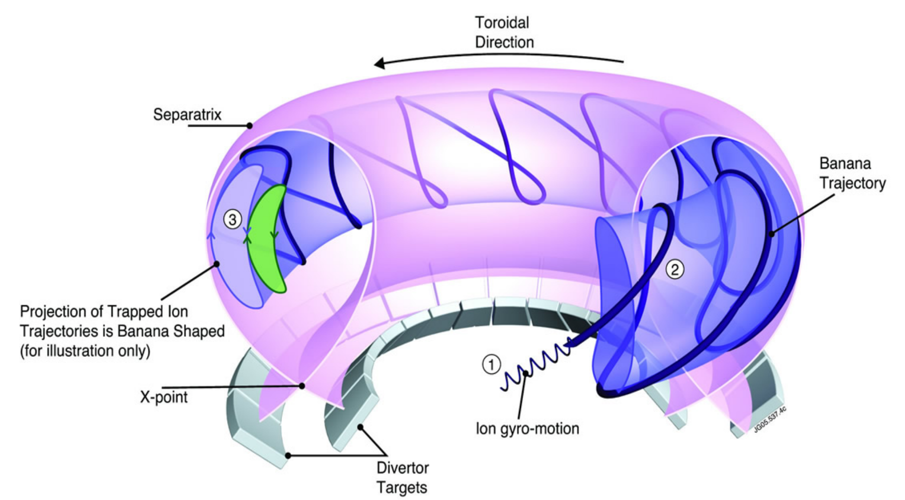

Image: EFDA-JET

Gyrokinetic Poisson (in long wavelength limit):

$$\nabla \cdot \left(\left[\lambda_D^2 \mathbf{I} + \lambda_L^2 \sum_i \frac{Z_i \bar{n}_i}{m_i \Omega_i^2} (\mathbf{I} - \mathbf{b}\mathbf{b}^T) \right] \nabla \Phi \right) = n_e - \sum_i Z_i \bar{n}_i$$

Polarization density

gyro-center ion density

$\mathbf{B}$ **Equilibrium magnetic field**

Φ **Equilibrium potential**

La **Larmor number (normalized gyroradius)**

$$\dot{\mathbf{R}} \equiv \frac{v_\parallel}{B_\parallel^*}\mathbf{B}^* + \frac{La}{ZB_\parallel^*}\mathbf{b} \times \mathbf{G} \qquad \dot{v}_\parallel \equiv -\frac{1}{mB_\parallel^*}\mathbf{B}^* \cdot \mathbf{G}$$

$$\mathbf{B}^* \equiv \mathbf{B} + La\frac{mv_\parallel}{Z}\nabla_R \times \mathbf{b} \qquad B_\parallel^* = \mathbf{b} \cdot \mathbf{B}^*$$

$$\mathbf{G} \equiv Z\nabla_R \Phi + \frac{\mu}{2}\nabla_R |\mathbf{B}| \qquad \mathbf{b} \equiv \mathbf{B}/|\mathbf{B}|$$

Some finite-Larmor radius effects are neglected

In 2D, a poloidal slice of the plasma edge is mapped to a multiblock, locally rectangular grid

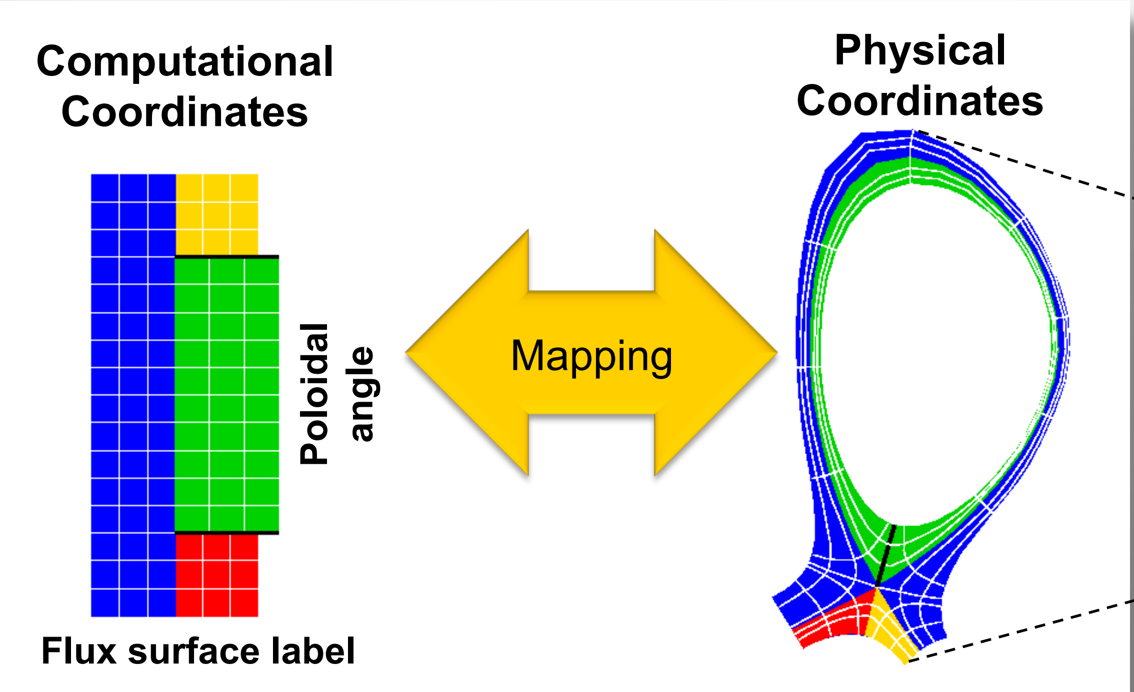

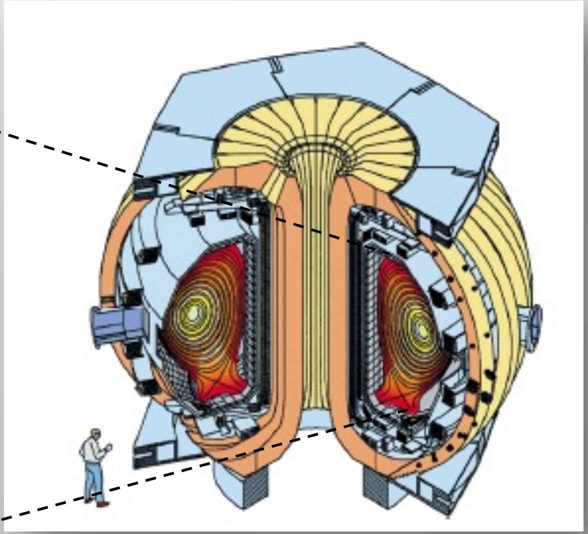

- Equilibrium magnetic field determines mapping from physical to computational coordinates
- Alignment with flux surfaces facilitates treatment of strong anisotropies
- Separatrix requires multiblock domain decomposition modified

We employ a systematic formalism for high-order, mapped-grid finite volume discretizations

Cartesian coordinates:

Spatial domain discretized as a union of rectangular control volumes

$$V_{\mathbf{i}} = \prod_{d=1}^{D} \left[i_d - \frac{h}{2}, i_d + \frac{h}{2} \right]$$

Mapped coordinates:

Smooth mapping from abstract Cartesian coordinates into physical space

$$\mathbf{X} = \mathbf{X}(\boldsymbol{\xi}), \qquad \mathbf{X} : [0,1]^D \rightarrow \mathbb{R}^D$$

Fourth-order flux divergence average from fourth-order cell face averages:

$$\int_{\mathbf{X}(V_{\mathbf{i}})} \nabla_{\mathbf{X}} \cdot \mathbf{F} d\mathbf{x} = \sum_{\pm=+,-} \sum_{d=1}^{D} \pm \int_{A_d^{\pm}} \left(\mathbf{N}^T \mathbf{F}\right)_d d\mathbf{A}_{\boldsymbol{\xi}} = h^{D-1} \sum_{\pm=+,-} \sum_{d=1}^{D} \pm F^d_{\mathbf{i}\pm\frac{1}{2}\mathbf{e}^d} + O\left(h^4\right)$$

where

$$\left(\mathbf{N}^T\right)_{p,q} = \det\left(\mathbf{R}_p\left(\frac{\partial \mathbf{X}}{\partial \boldsymbol{\xi}}, \mathbf{e}^q\right)\right)$$

$\mathbf{R}_p\left(\mathbf{A}, \mathrm{v}\right)$: replace p-th row of $\mathbf{A}$ with v

$$F^d_{\mathbf{i}\pm\frac{1}{2}\mathbf{e}^d} = \sum_{s=1}^{D} \langle N_d^s \rangle_{\mathbf{i}\pm\frac{1}{2}\mathbf{e}^d} \langle F^s \rangle_{\mathbf{i}\pm\frac{1}{2}\mathbf{e}^d} + \frac{h^2}{12} \sum_{s=1}^{D} \left(\mathbf{G}_0^{\perp,d}\left(\langle N_d^s \rangle_{\mathbf{i}\pm\frac{1}{2}\mathbf{e}^d}\right)\right) \cdot \left(\mathbf{G}_0^{\perp,d}\left(\langle F^s \rangle_{\mathbf{i}\pm\frac{1}{2}\mathbf{e}^d}\right)\right)$$

$\mathbf{G}_0^{\perp,d} =$ second-order accurate centered difference of $\nabla_{\boldsymbol{\xi}} - \mathbf{e}^d \frac{\partial}{\partial \xi_d}$

$$\langle q \rangle_{\mathbf{i}\pm\frac{1}{2}\mathbf{e}^d} \equiv \frac{1}{h^{D-1}} \int_{A_d} q(\boldsymbol{\xi}) d\mathbf{A}_{\boldsymbol{\xi}} + O\left(h^4\right)$$

[Colella, P. et al. (2011) *J. Comput. Phys.* **230** 2952-2976]

An important mapped grid stability requirement is the preservation of free streaming

Free streaming is preserved if :

$$\int_{\mathbf{X}(V_{\mathbf{i}})} \nabla_{\mathbf{X}} \cdot \mathbf{F} d\mathbf{x} = 0 \text{ for } \mathbf{F} \text{ constant}$$

This implies:

$$\int_V \nabla_\xi \cdot \mathbf{N}^T d\boldsymbol{\xi} = \sum_{+,-} \sum_{d=1}^{D} \pm \int_{\mathbf{A}_d^{\pm}} (\mathbf{N}^T)_d d\mathbf{A}_\xi = 0$$

Poincaré lemma tells us:

$$\exists \mathcal{M}^s_{d,d'} \quad d' \neq d \qquad \textbf{s.t.} \qquad N^s_d = \sum_{d' \neq d} \frac{\partial \mathcal{M}^s_{d,d'}}{\partial \xi_{d'}} \qquad \textbf{and} \qquad \mathcal{M}^s_{d,d'} = -\mathcal{M}^s_{d',d}$$

By Stokes' theorem:

$$\int_{A_d} N^s_d d\mathbf{A}_{\boldsymbol{\xi}} = \sum_{\pm=+,-} \sum_{d' \neq d} \pm \int_{E^{\pm}_d, d'} M^s_{d,d'} d\mathbf{E}_{\boldsymbol{\xi}}$$

So long as we consistently apply the same quadrature to the edge integrals, free-stream property is preserved

[Colella, P. et al. (2011) *J. Comput. Phys.* **230** 2952-2976]

Near the X point, field alignment must be abandoned to retain local mapping smoothness

- **Modified mappings cannot match smoothly at block boundaries**
- **To find the cell average of ϕ in a neighbor block ghost cell (centered at the red dot), assume a polynomial around the center:**

$$\phi(\xi) = \sum_p a_p \xi^p$$

- **Solve least squares system for coefficients**
- **Average interpolant over red cell**
- **Averaging of exchanged fluxes ensures strict conservation**

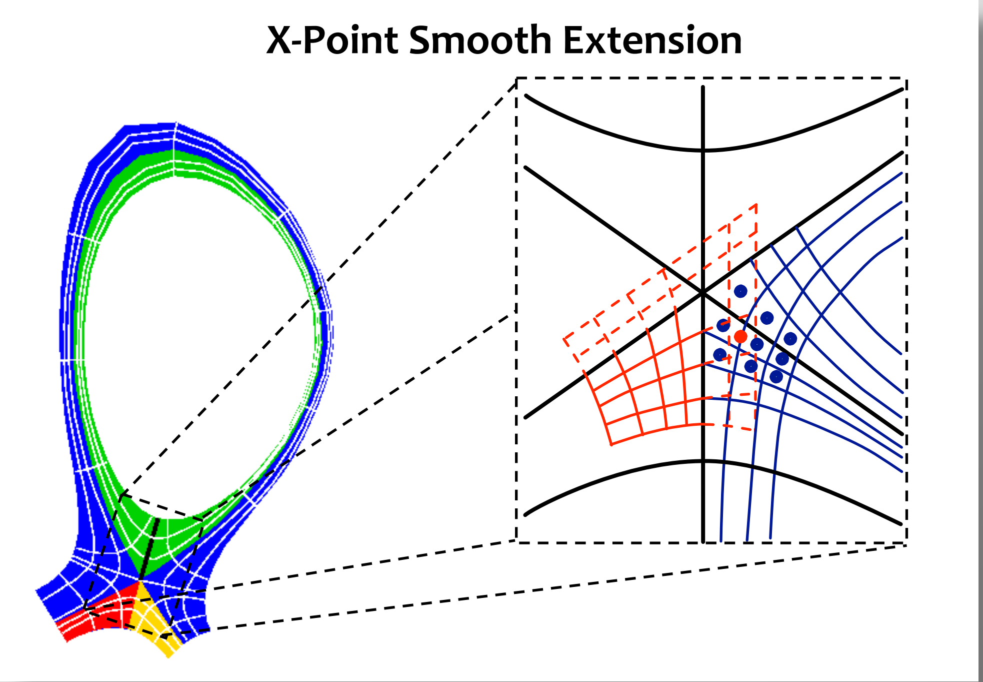

known for control volumes centered at blue dots

computable from (requires) red inverse mapping

$$\int_V \phi(\xi)d\xi = \sum_p a_p \int_V \xi^p(\xi)d\xi$$

[McCorquodale, P. Chombo Mapped Multiblock Desgin Document]

We use a fourth-order, limited, explicit method-of-lines discretization of the gyrokinetic Vlasov equation

- **Update of cell average:**

$$\frac{d\overline{(uJ)}_{\mathbf{i}}}{dt} \approx -\frac{1}{h}\sum_{d=1}^{D}\left(F^d_{\mathbf{i}+\frac{1}{2}\mathbf{e}^d} - F^d_{\mathbf{i}-\frac{1}{2}\mathbf{e}^d}\right)$$

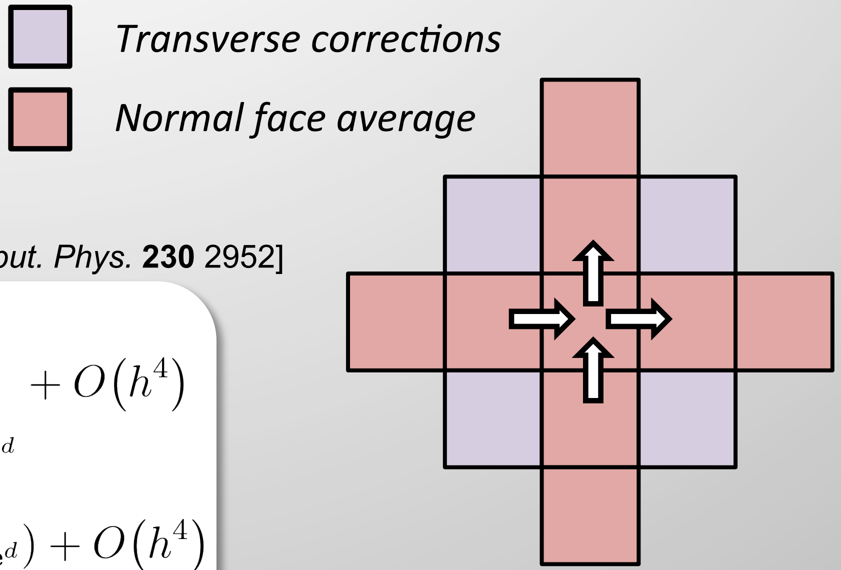

- **Face-averaged flux:** [Colella *et al.* (2011) *J. Comput. Phys.* **230** 2952]

$$\langle \mathbf{F}\rangle_{\mathbf{i}+\frac{1}{2}\mathbf{e}^d} = \left(\langle \mathbf{v}\rangle\langle u\rangle + \frac{h^2}{12}\sum_{d'\neq d}\frac{\partial \mathbf{v}}{\partial \xi_{d'}}\frac{\partial u}{\partial \xi_{d'}}\right)_{\mathbf{i}+\frac{1}{2}\mathbf{e}^d} + O(h^4)$$

$$\langle u\rangle_{\mathbf{i}+\frac{1}{2}\mathbf{e}^d} = \frac{7}{12}\left(\overline{u}_{\mathbf{i}+\mathbf{e}^d} + \overline{u}_{\mathbf{i}}\right) - \frac{1}{12}\left(\overline{u}_{\mathbf{i}+2\mathbf{e}^d} + \overline{u}_{\mathbf{i}-\mathbf{e}^d}\right) + O(h^4)$$

- **Standard explicit four-stage, fourth-order Runge-Kutta in time**
- **We have additional nonlinear options:**
  - **Extremum-preserving PPM limiting** [McCorquodale and Colella (2011) *CAMCoS* **6** 1]
  - **WENO-like upwind limiting** [Banks and Hittinger (2010) *IEEE T. Plasma Sci* **38** 9]
  - **FCT positivity-preservation** [Zalesak (1979) *J. Comput. Phys* **35** 335]
  - **Local redistribution positivity-preservation** [Hilditch and Colella (1997) AIAA-1997-263]

WENO-like scheme: Fluxes nonlinearly suppressed with minimal numerical dissipation

- At each face, compute two third-order interpolants:

$$\langle f\rangle^L_{\mathbf{i}+\frac{1}{2}\mathbf{e}^d} = \left[-\bar{f}_{\mathbf{i}-\mathbf{e}^d} + 5\bar{f}_{\mathbf{i}} + 2\bar{f}_{\mathbf{i}+\mathbf{e}^d}\right]/6$$

$$\langle f\rangle^R_{\mathbf{i}+\frac{1}{2}\mathbf{e}^d} = \left[2\bar{f}_{\mathbf{i}} + 5\bar{f}_{\mathbf{i}+\mathbf{e}^d} - \bar{f}_{\mathbf{i}+2\mathbf{e}^d}\right]/6$$

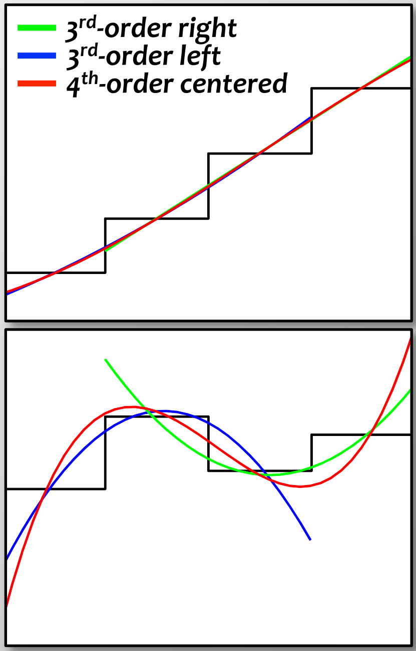

- Face average is the weighted average, with weights based on a measure of local smoothness:

$$\langle f\rangle_{\mathbf{i}+\frac{1}{2}\mathbf{e}^d} = w^L_{\mathbf{i}+\frac{1}{2}\mathbf{e}^d}\langle f\rangle^L_{\mathbf{i}+\frac{1}{2}\mathbf{e}^d} + w^R_{\mathbf{i}+\frac{1}{2}\mathbf{e}^d}\langle f\rangle^R_{\mathbf{i}+\frac{1}{2}\mathbf{e}^d}$$

- In smooth regions, one obtains the fourth-order centered average:

$$\langle f\rangle_{\mathbf{i}+\frac{1}{2}\mathbf{e}^d} = \frac{7}{12}\left(\bar{f}_{\mathbf{i}} + \bar{f}_{\mathbf{i}+\mathbf{e}^d}\right) - \frac{1}{12}\left(\bar{f}_{\mathbf{i}-\mathbf{e}^d} + \bar{f}_{\mathbf{i}+2\mathbf{e}^d}\right) + O\left(h^4\right)$$

- In non-smooth regions, bias towards the upwind stencil introduces additional numerical dissipation

[Banks & Hittinger, *IEEE Trans Plasma Sci* 38 (2010) 2198-2207]

We use nonlinear weights that are a variant of the WENO approach

Curvatures

$$A^L_{\mathbf{i}+\frac{1}{2}\mathbf{e}^d} = \Delta^d_+ \Delta^d_- \bar{f}_{\mathbf{i}}$$

$$A^R_{\mathbf{i}+\frac{1}{2}\mathbf{e}^d} = \Delta^d_+ \Delta^d_- \bar{f}_{\mathbf{i}+\mathbf{e}^d}$$

Central Slopes

$$B^L_{\mathbf{i}+\frac{1}{2}\mathbf{e}^d} = \left(\Delta^d_+ + \Delta^d_-\right) \bar{f}_{\mathbf{i}}$$

$$B^R_{\mathbf{i}+\frac{1}{2}\mathbf{e}^d} = \left(\Delta^d_+ + \Delta^d_-\right) \bar{f}_{\mathbf{i}+\mathbf{e}^d}$$

Smoothness Detectors

$$\beta^L_{\mathbf{i}+\frac{1}{2}\mathbf{e}^d} = \left[\frac{4}{3}A^2 + \frac{1}{2}AB + \frac{1}{4}B^2\right]^L_{\mathbf{i}+\frac{1}{2}\mathbf{e}^d}$$

$$\beta^R_{\mathbf{i}+\frac{1}{2}\mathbf{e}^d} = \left[\frac{4}{3}A^2 - \frac{1}{2}AB + \frac{1}{4}B^2\right]^R_{\mathbf{i}+\frac{1}{2}\mathbf{e}^d}$$

$$a^{L,R}_{\mathbf{i}+\frac{1}{2}\mathbf{e}^d} = \frac{1}{2}\left[\epsilon + \beta^{L,R}_{\mathbf{i}+\frac{1}{2}\mathbf{e}^d}\right]^{-2}$$

$$c^{L,R}_{\mathbf{i}+\frac{1}{2}\mathbf{e}^d} = \left[\frac{a^{L,R}}{a^L + a^R}\right]_{\mathbf{i}+\frac{1}{2}\mathbf{e}^d}$$

Assign larger to *upwind* weight

$$w^L_{\mathbf{i}+\frac{1}{2}\mathbf{e}^d} = \begin{cases} \max\left(c^L, c^R\right) & \text{if } u^d_{\mathbf{i}+\frac{1}{2}\mathbf{e}^d} > 0 \\ \min\left(c^L, c^R\right) & \text{otherwise} \end{cases}$$

$$w^R_{\mathbf{i}+\frac{1}{2}\mathbf{e}^d} = 1 - w^L_{\mathbf{i}+\frac{1}{2}\mathbf{e}^d}$$

Can further condition weights to get optimal rates near certain critical points

[Henrick, Aslam & Powers, *J Comput Phys* 207 (2005) 542-567]

We have demonstrated fourth-order convergence with our advection scheme even across severe block boundaries

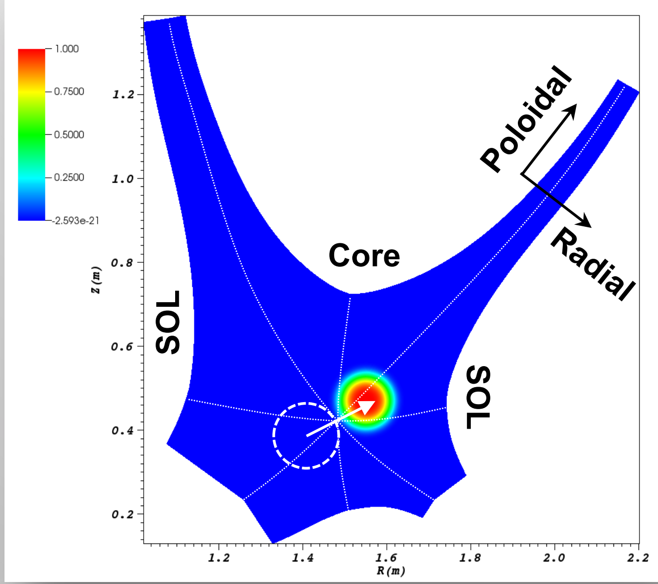

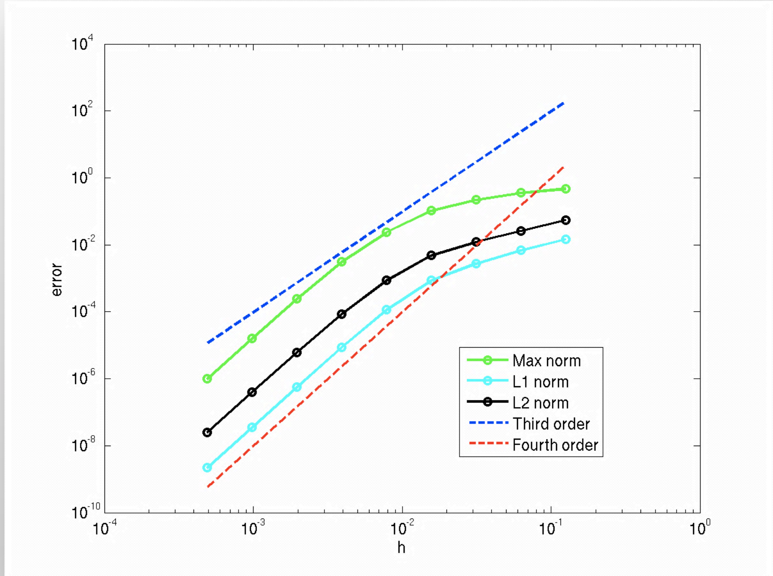

- Constant linear advection in configuration space through the X-point in 2D
- Non-axisymmetric in order to compare with analytic solution
- Grid convergence study across 9 resolutions by factor of 2

Domain	Resolution Sequence
Poloidal (in each block)	4, 8,..., 1024
Core Radial	8, 16,..., 2048
SOL Radial	12, 24,..., 3072

We use an analogous discretization of the gyrokinetic Poisson equation

- **Poisson in Finite-Volume:**

$$\nabla_X^2 \phi = \nabla_\xi \cdot \mathbf{C} \nabla_\xi \phi = \bar{\rho}_{\mathbf{i}} \quad \Rightarrow \quad \frac{1}{h} \sum_{d=1}^{D} \left(F^d_{\mathbf{i}+\frac{1}{2}\mathbf{e}^d} - F^d_{\mathbf{i}-\frac{1}{2}\mathbf{e}^d} \right) = \bar{\rho}_{\mathbf{i}}$$

$$\mathbf{C} = J^{-1} \mathbf{N}^T \mathbf{N}$$

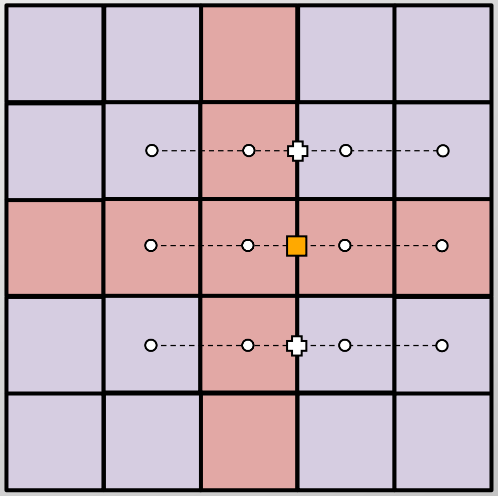

- **Face-averaged flux:** [Colella *et al.* (2011) *J. Comput. Phys.* **230** 2952]

$$F^d_{\mathbf{i}+\frac{1}{2}\mathbf{e}^d} \approx \sum_{d'=1}^{3} \left[\langle \mathbf{C} \rangle_{dd'} \left\langle \frac{\partial \phi}{\partial \xi_{d'}} \right\rangle + \frac{h^2}{12} \sum_{d'' \neq d} \frac{\partial \mathbf{C}}{\partial \xi_{d''}} \cdot \frac{\partial}{\partial \xi_{d''}} \left(\frac{\partial \phi}{\partial \xi_{d'}} \right) \right]_{\mathbf{i}+\frac{1}{2}\mathbf{e}^d}$$

- **For example, for** $d = d'$

$$\left\langle \frac{\partial \phi}{\partial \xi_d} \right\rangle_{\mathbf{i}+\frac{1}{2}\mathbf{e}^d} = \frac{1}{h} \left[\beta_{\mathbf{i}+\frac{1}{2}\mathbf{e}^d} + \frac{1}{24} \sum_{d' \neq d} \left(\beta_{\mathbf{i}+\frac{1}{2}\mathbf{e}^d + \mathbf{e}^{d''}} - 2\beta_{\mathbf{i}+\frac{1}{2}\mathbf{e}^d} + \beta_{\mathbf{i}+\frac{1}{2}\mathbf{e}^d - \mathbf{e}^{d''}} \right) \right] + O\left(h^4\right)$$

$$\beta_{\mathbf{i}+\frac{1}{2}\mathbf{e}^d} = \frac{1}{24} \left[27 \left(\phi_{\mathbf{i}+\mathbf{e}^d} - \phi_{\mathbf{i}} \right) - \left(\phi_{\mathbf{i}+2\mathbf{e}^d} - \phi_{\mathbf{i}-\mathbf{e}^d} \right) \right]$$

We solve the resulting system using a preconditioned Krylov method with an algebraic multigrid preconditioner

Evaluate as a mapped grid divergence

$$\nabla \cdot (\mathbf{D} \cdot \nabla \phi) = r$$

$\mathbf{D}$: tensor

$\mathbf{F} = \mathbf{D} \cdot \nabla \phi$: flux

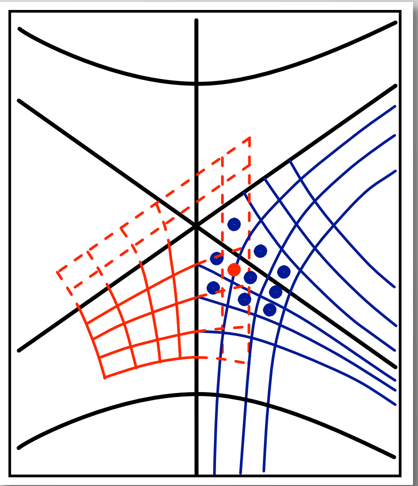

- Use either BiCGStab or GMRES
  - Matrix-vector multiplication re-uses mapped grid divergence
- Preconditioner: Algebraic multigrid
  - Applied to second-order discretization
  - Semi-structured *hypre* interface
  - Matrices & vectors constructed in two steps
    1. Structured stencil: Regular couplings within blocks, e.g. a nine-point stencil
    2. Unstructured stencil: Sparse couplings at interblock boundaries
  - Stencil indices and weights are exchanged across block boundaries

COGENT predictions of Geodesic Acoustic Mode (GAM) frequencies and damping rates agree well with theory

- **Geodesic Acoustic Mode: an eigenmode of the gyrokinetic Vlasov-Poisson system in toroidal geometry**
- **Kinetic effects cause collisionless damping**
- **Frequencies and damping rates predicted from a theoretical dispersion analysis**

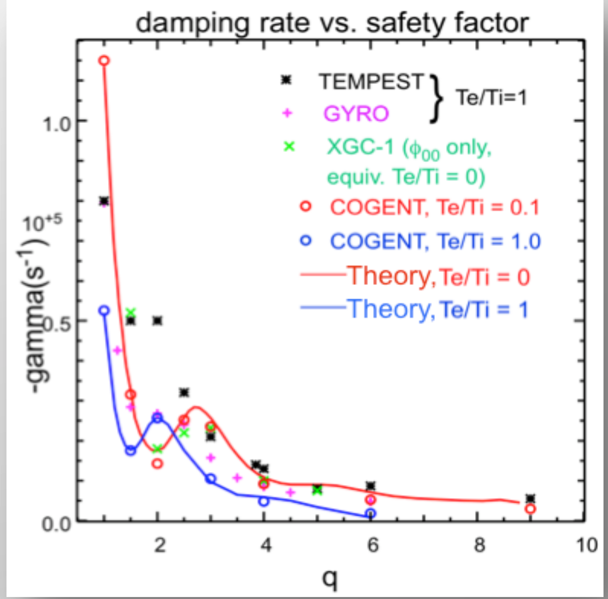

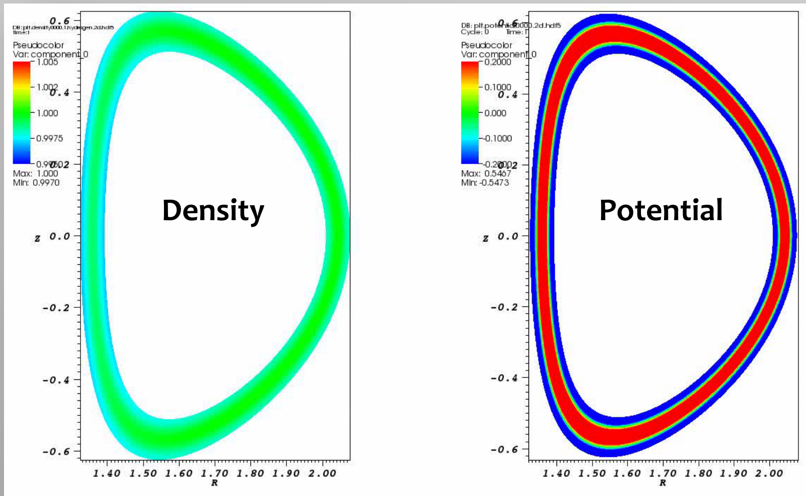

- **Tests involved parameter scans of**
  - **q = field line pitch ("safety factor")**
  - **T_e/T_i = electron/ion temperature ratio**

[Dorr, M. R. *et al.* (2010) *Proc. SciDAC 2010*]

Comparison of GAM runs at varying phase space resolution displays fourth-order convergence

Grid refinement level (N)	Grid (radial x poloidal x vparallel x mu)	Estimated density error conv. rate (r)	Richardson extrapolated density error (e)
1	8 x 32 x 32 x 8		
2	16 x 64 x 64 x 16		
3	32 x 128 x 128 x 32	3.8 (L1) 3.8 (L2) 4.1 (Max)	3.37×10^{-7} (L1) 6.03×10^{-7} (L2) 1.95×10^{-4} (Max)
4	64 x 256 x 256 x 64	4.2 (L1) 4.1 (L2) 3.6 (Max)	1.40×10^{-8} (L1) 2.95×10^{-7} (L2) 1.69×10^{-5} (Max)

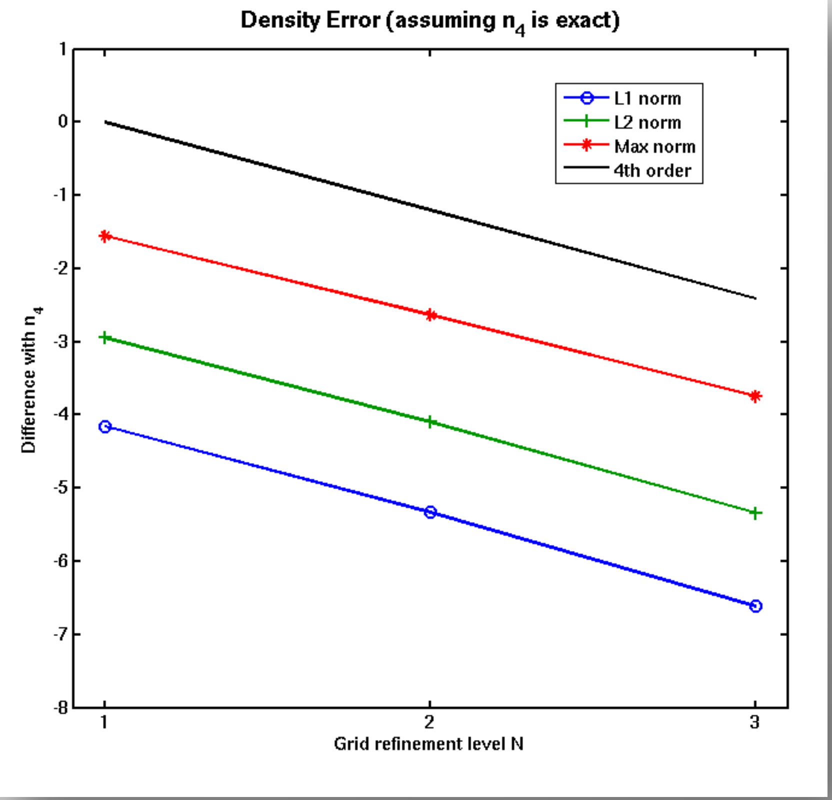

n_i = density at refinement level i

$d_i = || n_{i+1} - n_i ||_{x},\quad x = L1, L2, Max$

Rate estimate: $r = \log(d_{i+1}/d_i) / \log(2)$

Error estimate: $e = \log(d_i) / (1 + 2^r)$

Solution of the GKPoisson-Boltzmann equation on closed flux surfaces requires careful preconditioning

Solving

$$F(\Phi) = -\nabla \cdot N^T \left[(De)^2 \mathbf{I} + \frac{(La)^2}{B^2} \sum_i Z_i m_i \bar{n}_i \left(\mathbf{I} - \mathbf{b}\mathbf{b}^\mathbf{T} \right) \right] N J^{-1} \nabla \Phi + \frac{\langle \sum_i Z_i \bar{n}_i \rangle}{\langle \exp(\Phi/T_e) \rangle} \exp(\Phi/T_e) - \sum_i Z_i \bar{n}_i = 0$$

$\langle \cdot \rangle$ = average over *j*-th flux surface

via Newton iteration requires a linear Jacobian system solve with the non-symmetric matrix

$$J \equiv G + M(I - PD)$$

where

$$G \equiv -\nabla \cdot N^T \left[(De)^2 \mathbf{I} + \frac{(La)^2}{B^2} \sum_i Z_i m_i \bar{n}_i \left(\mathbf{I} - \mathbf{b}\mathbf{b}^\mathbf{T} \right) \right] N J^{-1} \nabla$$

$$M \equiv \frac{\langle \sum_i Z_i \bar{n}_i \rangle}{T_e \langle \exp(\Phi/T_e) \rangle} \exp(\Phi/T_e)$$

$$D \equiv \frac{\exp(\Phi/T_e)}{\langle \exp(\Phi/T_e) \rangle}$$

$P \equiv$ projection onto vectors that are constant along flux surfaces

To solve *Jz = r*, premultiply by *M*$^{-1}$ and project onto orthogonal subspaces:

$$\begin{aligned} P\left(M^{-1}G + I - D\right) z &= P M^{-1} r, \\ (I-P)\left(M^{-1}G + I\right) z &= (I-P) M^{-1} r \end{aligned}$$

Assume $(I-P)M^{-1}G \approx 0.$ **Then**

$$z = Pz + (I-P)M^{-1} r$$

where *Pz* is the solution of the 1D system

$$\begin{aligned} &P\left(M^{-1}G + I - D\right) Pz \\ &= P\left[I - \left(M^{-1}G + I - D\right)(I-P)\right] M^{-1} r \end{aligned}$$

This solver strategy is working well (so far)

Divergence cleaning solve:

$$\Delta\phi = \nabla \cdot \mathbf{B}$$

- PCG
- Preconditioner: 2 BoomerAMG V-cycles with 2nd order operator

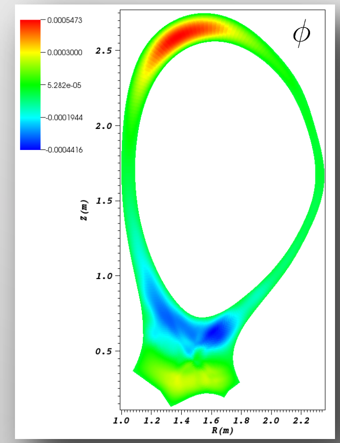

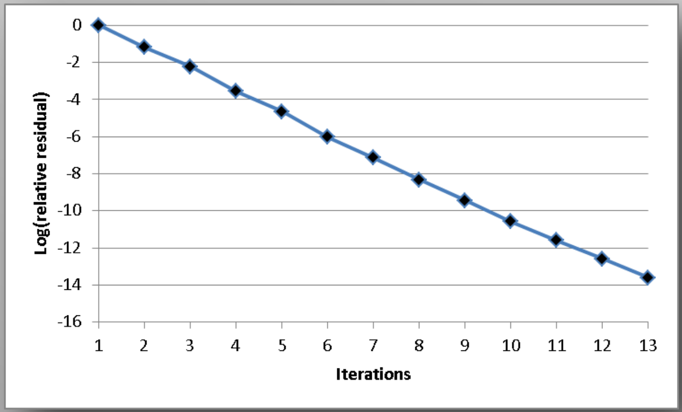

GKPoisson solve:

$$\nabla \cdot \left(\left[\lambda_D^2 \mathbf{I} + \lambda_L^2 \sum_i \frac{Z_i \bar{n}_i}{m_i \Omega_i^2} (\mathbf{I} - \mathbf{b}\mathbf{b}^T) \right] \nabla \Phi \right) = n_e - \sum_i Z_i \bar{n}_i$$

- PCG
- Preconditioner: 1 BoomerAMG V-cycle with 2nd order operator

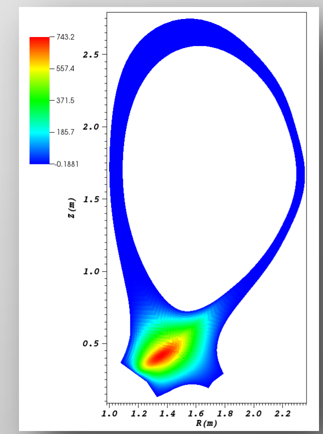

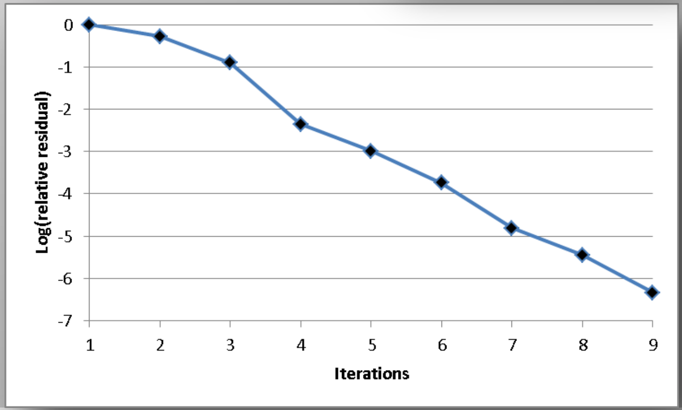

We have employed a divergence cleaning process to fix experimentally-derived geometric data

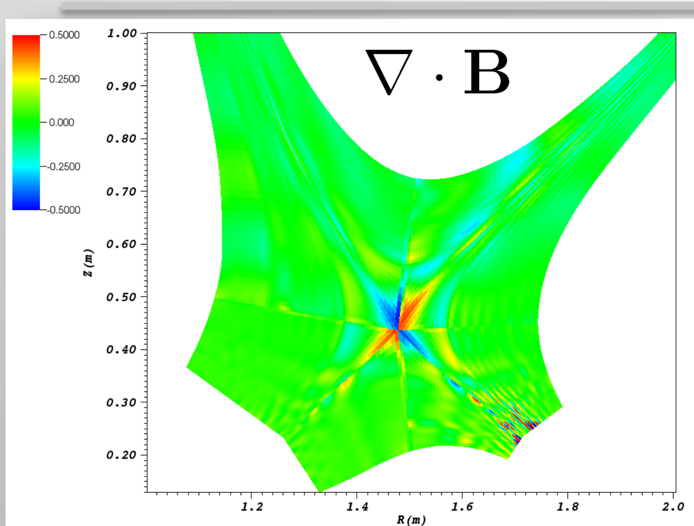

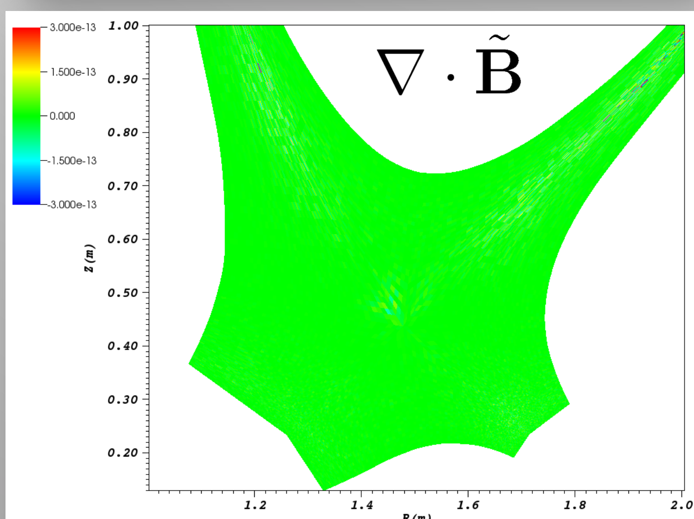

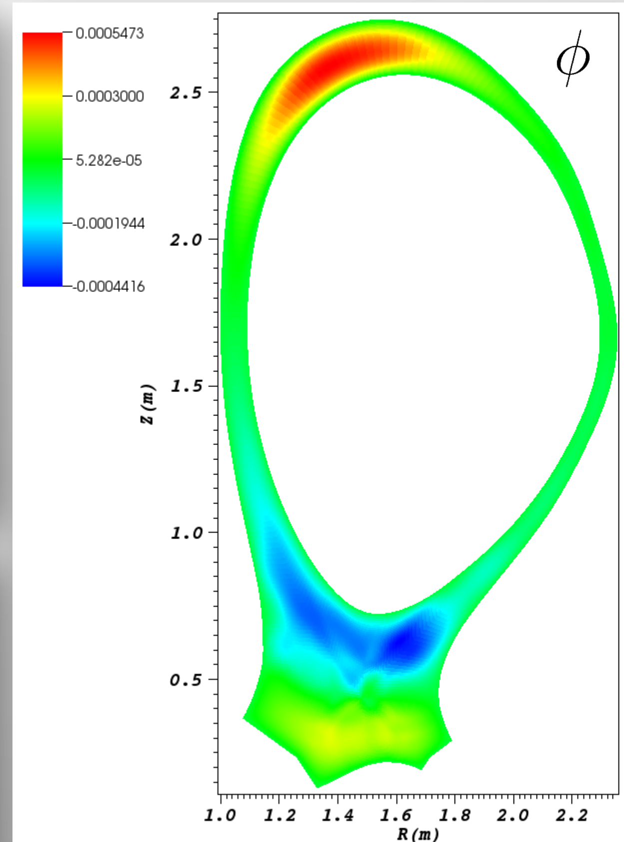

- Geometry based on measured B-field from DIII-D tokamak
- Discrete data violates divergence-free gyrokinetic velocity
- Worst at X-point
- Enforce B-field divergence by solving:

$$\nabla^2 \phi = \nabla \cdot \mathrm{B}$$
$$\tilde{\mathrm{B}} = \mathrm{B} - \nabla \phi$$

- **Solved using the same Poisson-solve strategy:**
  - PCG iteration using mapped grid divergence operator for matrix-vector multiplications
  - hypre BoomerAMG solver preconditioner

We have begun to run tests on more physically-relevant test problems, such as the "Loss Cone"

- **Initial Condition:**

$$f_0(\mathbf{R}, v_\parallel, \mu) = \pi^{3/2} \exp\left(-v_\parallel^2 - \frac{B(\mathbf{R})\mu}{2}\right)$$

- **Boundary Conditions: characteristic with**

$$f_{\text{in}}(\mathbf{R}, v_\parallel, \mu, t) = \begin{cases} 0, & \text{external} \\ f_0(\mathbf{R}, v_\parallel, \mu), & \text{core} \end{cases}$$

- **512 cores on LLNL cab (43.5TF Intel Xeon)**

Domain	Resolution
Left/Right Core	16 x 128 x 64 x 64
Central SOL	24 x 128 x 64 x 64
Left/Right SOL	12 x 32 x 64 x 64
Left/Right Private Flux	24 x 32 x 64 x 64

Single null geometry decomposition

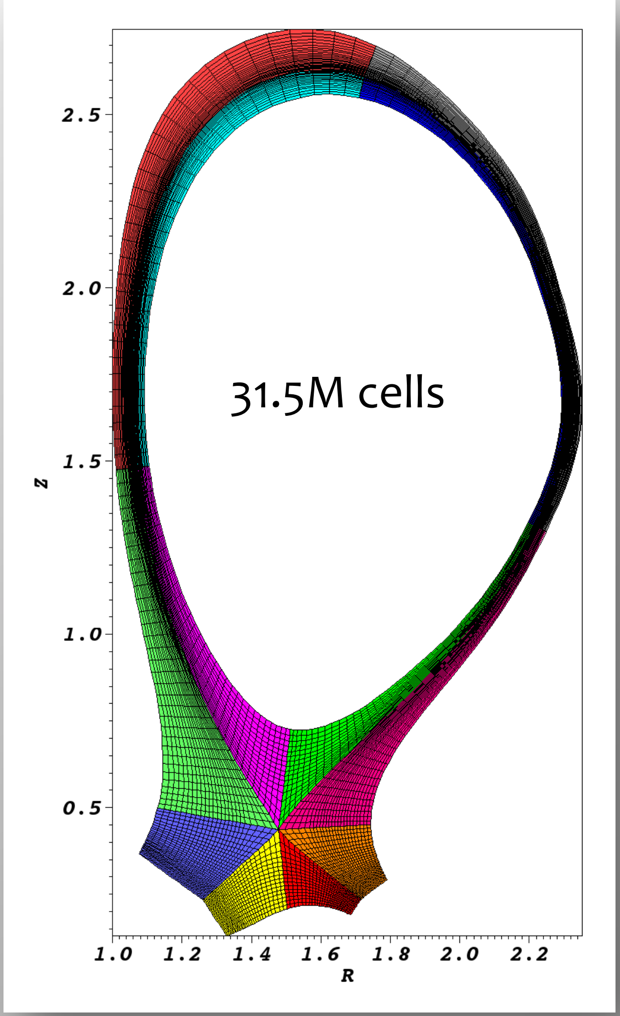

After nearly 7500 steps, the solution approaches a non-Maxwellian steady state near the separatrix

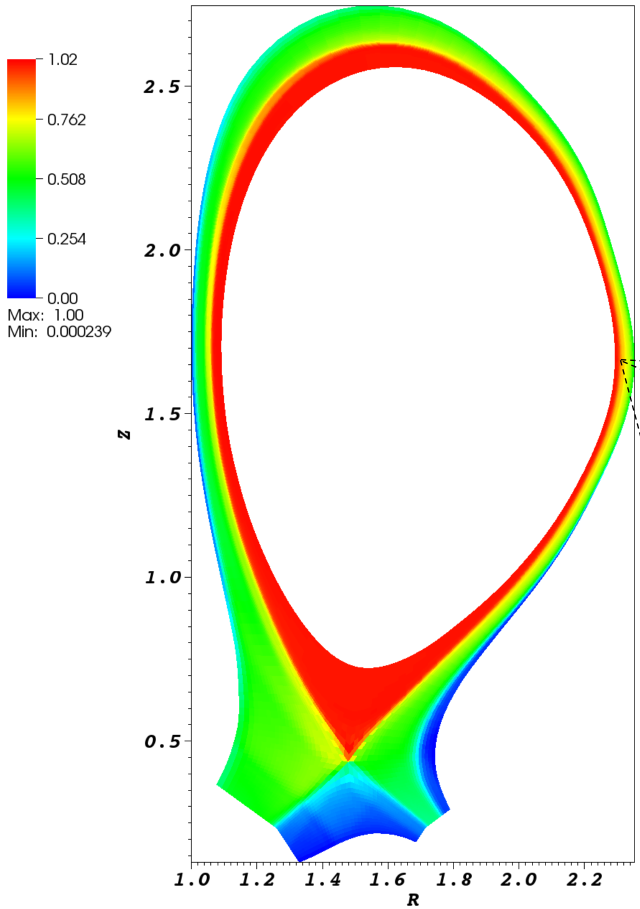

Density

- Physical explanation:
  - Advection in phase space
  - Open field lines carry particles into diverter plates
  - Density depletes in SOL

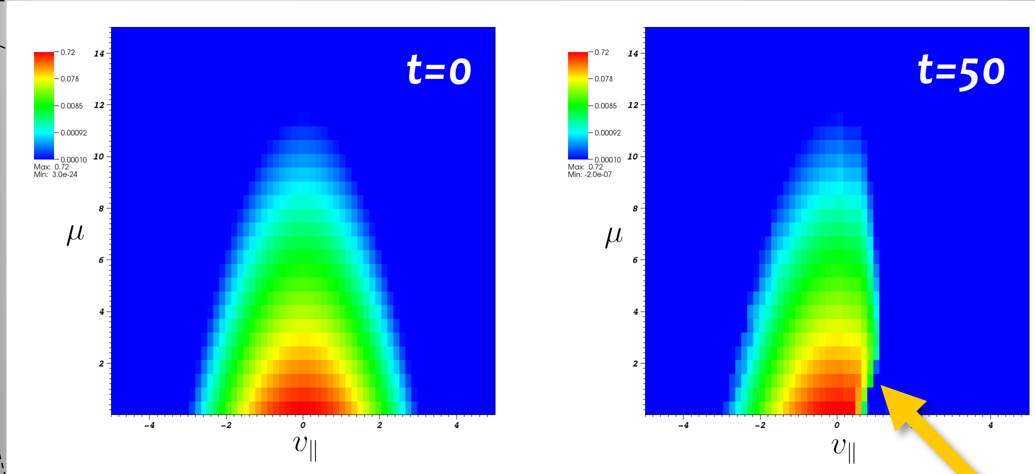

Magnetic well traps particles ("banana" orbits), so loss boundary is curved

COGENT has been refactored to accommodate an IMEX time integrator for collisions

- **Consider semi-discrete problem with stiff and non-stiff terms:**

$$\frac{du_i}{dt} = F_E(u_i) + F_I(u_i)$$

- **General additive partitioned ARK$_2$ scheme**

$$\left(u^{(s)} - \Delta t \gamma F_I(u^{(s)})\right) = u^n + \Delta t \sum_{j=1}^{s-1} \left[a_{s,j}^{[E]} F_E(u^{(j)}) + a_{s,j}^{[I]} F_I(u^{(j)})\right]$$
$$u^{n+1} = u^{(s)} + \Delta t \sum_{j=1}^{s} (b_j - a_{s,j}^{[E]}) F_E(u^{(j)})$$

- **ARK4(3)6L[2]SA of Kennedy and Carpenter**
  - Combines 4th-order Explicit RK with 4th--order Explicit Singly Diagonally Implicit RK
  - ESDIRK advantages: L-stability, stiff accuracy, stage order of two
  - Suffers from order-reduction in transition between stiff and non-stiff limits
  - Chombo provides an interface with dense output for time refinement
- **With this framework, can try other IMEX RK schemes as well**

AMR in phase space has the potential to significantly reduce the amount of mesh required

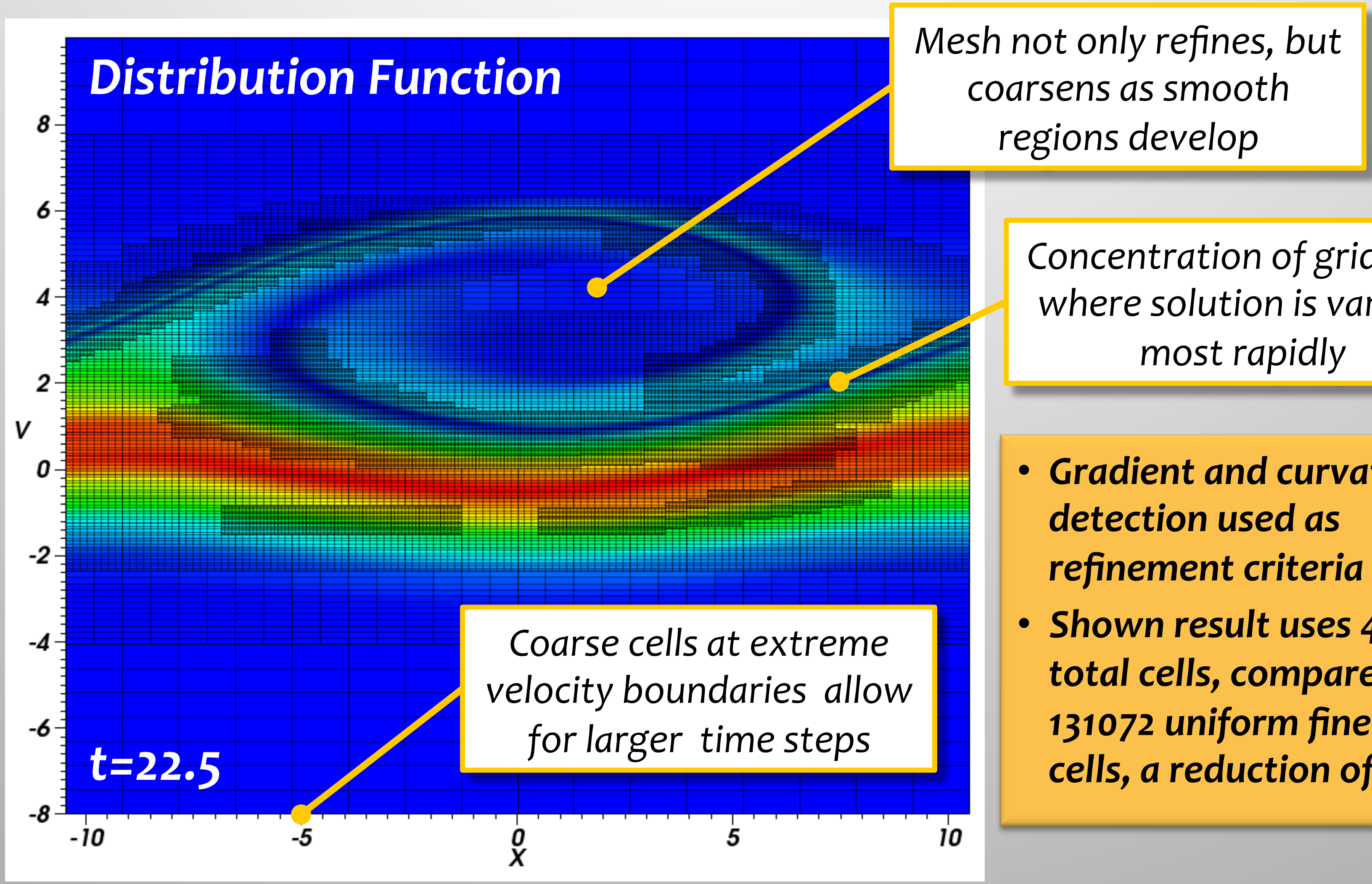

- ***Gradient and curvature detection used as refinement criteria***
- ***Shown result uses 40784 total cells, compared to 131072 uniform fine-grid cells, a reduction of 69%.***

Adaptive mesh refinement (AMR) in multiple dimensions introduces several new challenges

- Our approach is a block-structured formulation
  - Arbitrary refinement
  - Arbitrary parallel decomposition
  - Known path to local time refinement
- High-order discretizations require conservative, high-order interpolation operators
- Communications between dimensions require efficient:
  - Reduction
  - Injection
  - Hierarchy sychronization

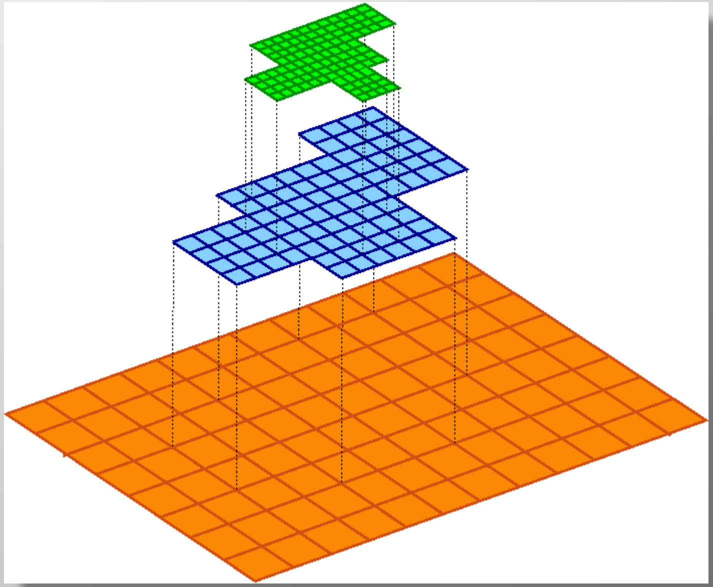

Principal challenge with AMR is communicating between mesh hierarchies of differing dimensions

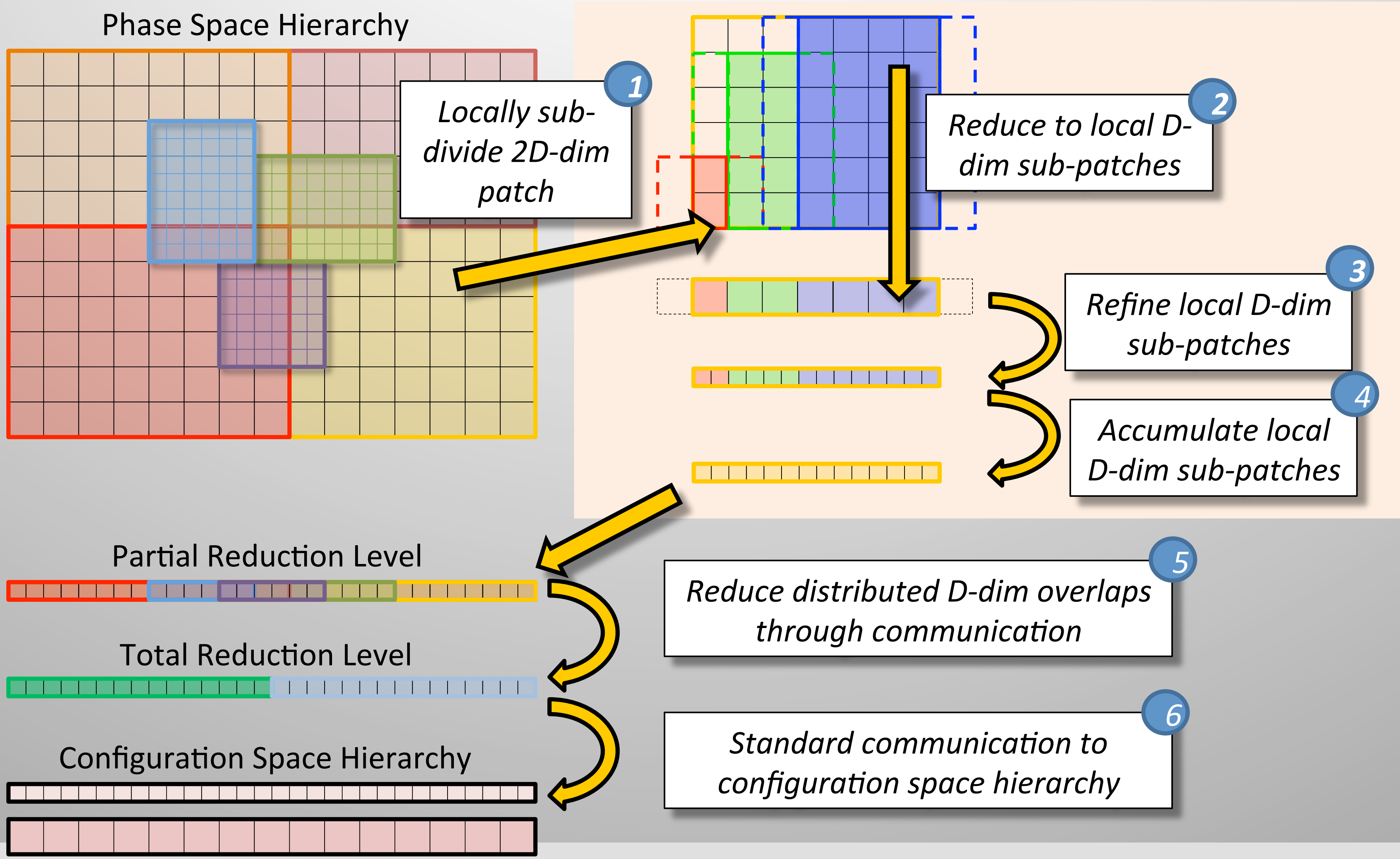

Distribution function for Bump-On-Tail simulation demonstrating AMR (gradient refinement criteria)

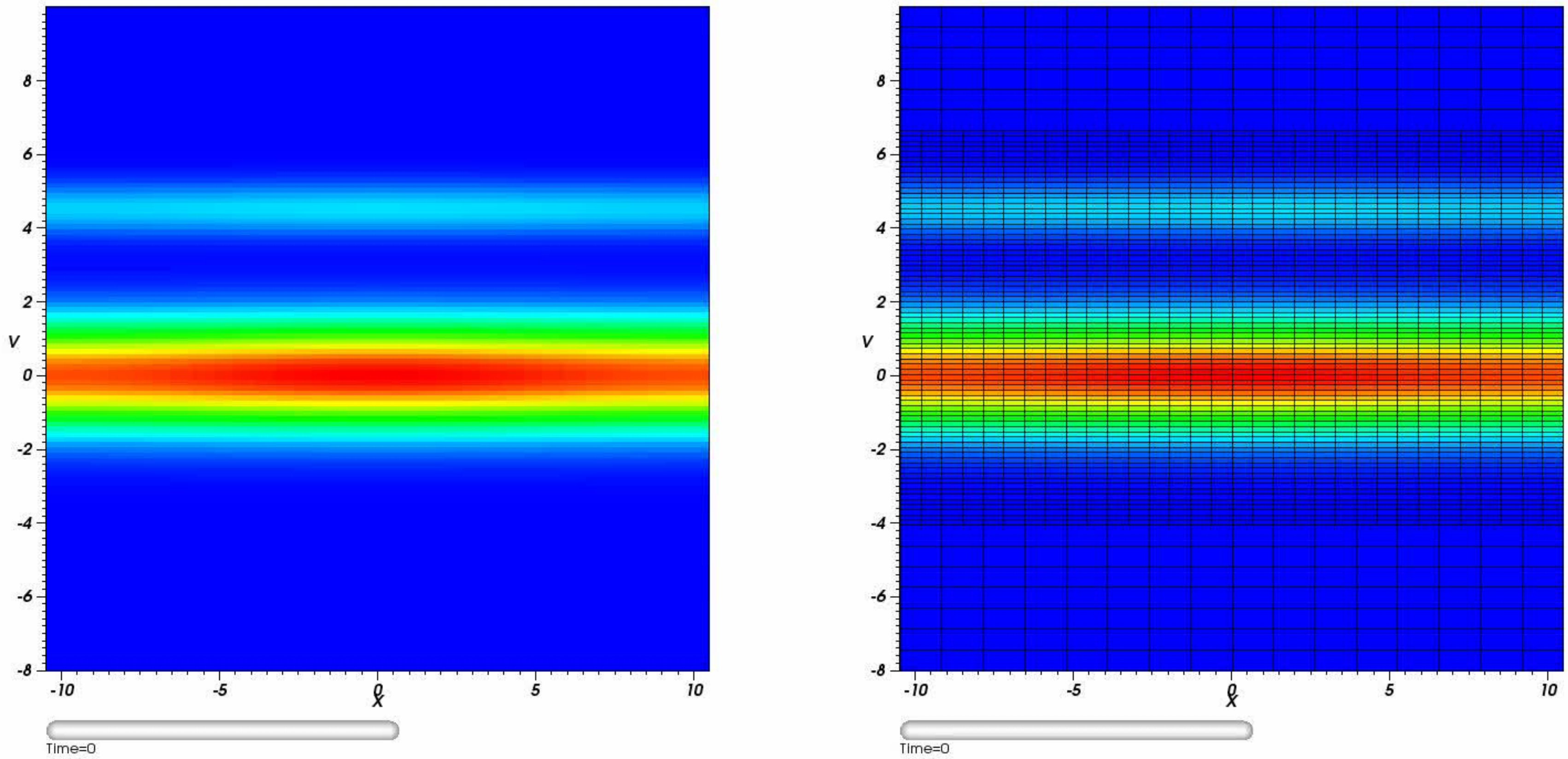

$$f_0(x,v) = [(1+0.04\cos(0.3x)]f_b(v)$$

$$f_b(v) = \frac{0.9}{\sqrt{2\pi}}\exp\left[-\frac{v^2}{2}\right] + \frac{0.2}{\sqrt{2\pi}}\exp\left[-4(v-4.5)^2\right]$$

AMR can reproduce uniform grid results, but speed-up is sensitive to AMR parameters

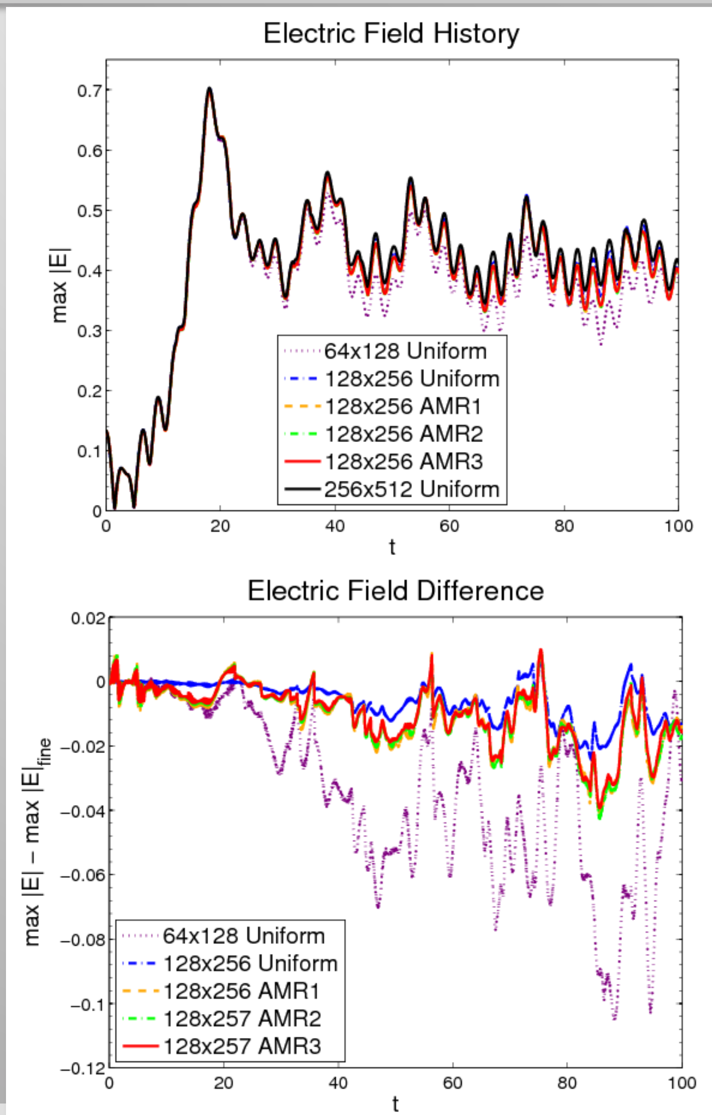

Case	Avg Time (s)	AMR Speed-Up
Uniform	1520	1.00
AMR1	2623	0.58
AMR2	1346	1.13
AMR3	960	1.58

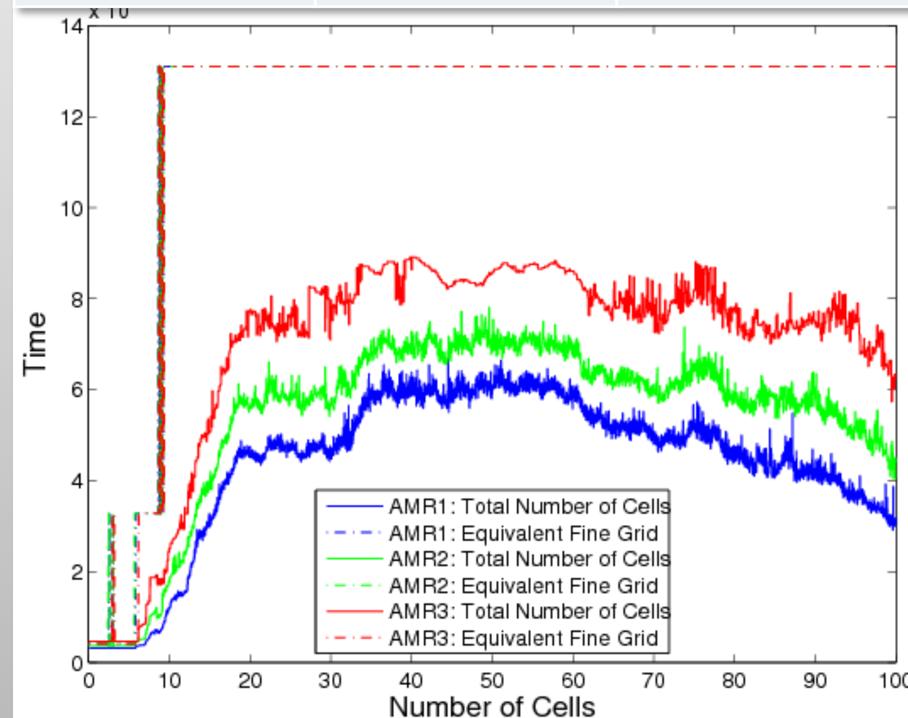

[Hittinger & Banks, JCP 241 (2013) 118-140]

Gyrokinetic simulation of the edge imposes challenges that require many technologies working together

- **We have most of these technologies working in concert**
- **Next steps:**
  - **Self-consistent Vlasov-Poisson problems**
  - **Meshing smoothness**
  - **Collisions**
  - **Finite Larmor radius**
  - **BCs**
  - **AMR**

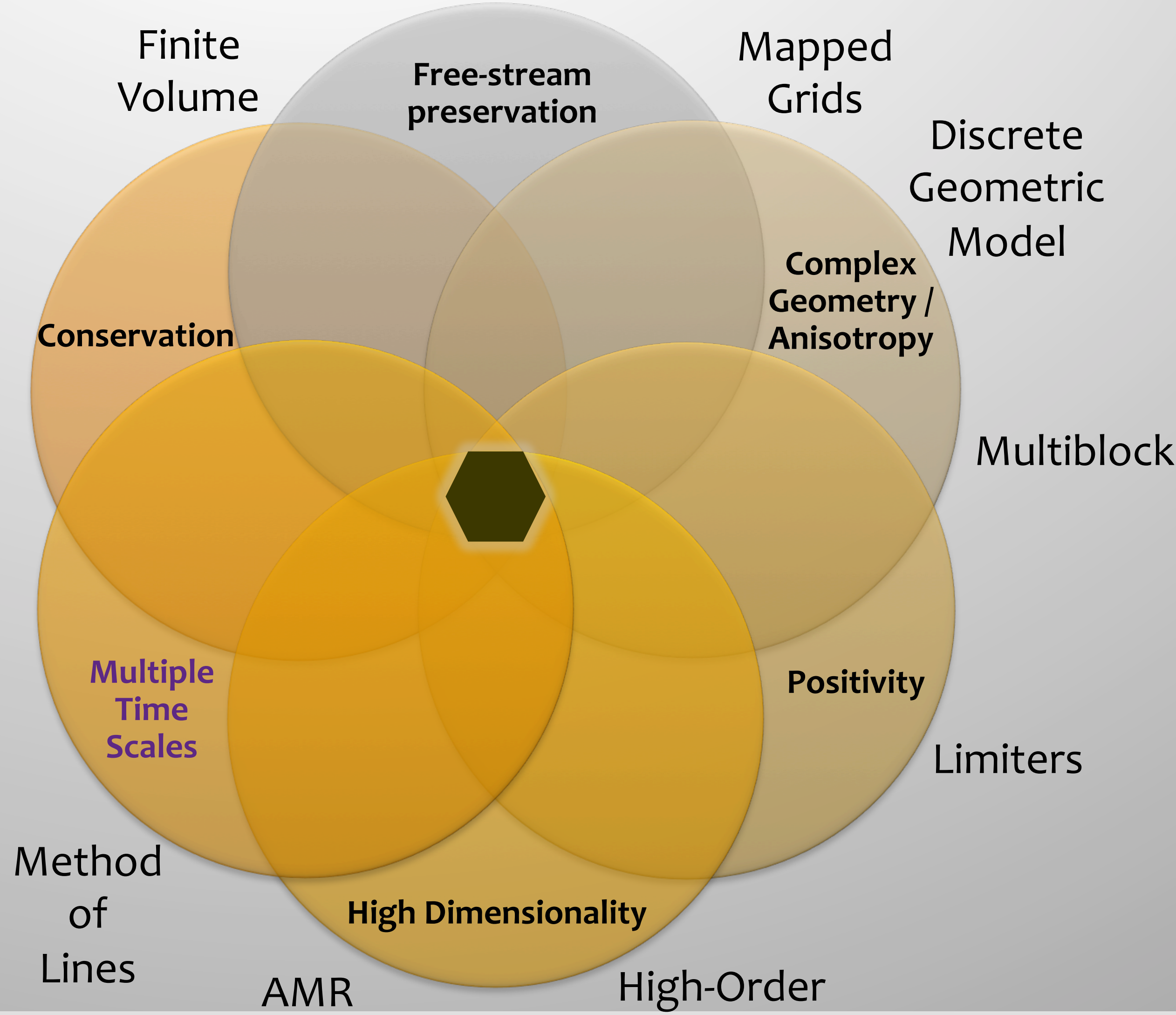

Lawrence Livermore National Laboratory